Random Body Movement Cancellation in Doppler Radar Vital Sign Detection

Changzhi Li, *Student Member, IEEE*, and Jenshan Lin, *Senior Member, IEEE*

***Abstract*—The complex signal demodulation and the arctangent demodulation are studied for random body movement cancellation in quadrature Doppler radar noncontact vital sign detection. This technique can be used in sleep apnea monitor, lie detector, and baby monitor to eliminate the false alarm caused by random body movement. It is shown that if the dc offset of the baseband signal is accurately calibrated, both demodulation techniques can be used for random body movement cancellation. While the complex signal demodulation is less likely to be affected by a dc offset, the arctangent demodulation has the advantage of eliminating harmonic and intermodulation interference at high carrier frequencies. When the dc offset cannot be accurately calibrated, the complex signal demodulation is more favorable. Ray-tracing model is used to show the effects of constellation deformation and optimum/null detection ambiguity caused by the phase offset due to finite antenna directivity. Experiments have been performed using 4–7 GHz radar to verify the theory.**

***Index Terms*—Arctangent demodulation, complex signal demodulation, dc offset, noncontact, phase offset, random body movement cancellation, ray tracing, vital sign, wireless.**

I. Introduction

REMOTE noncontact detection of vital signs, i.e., the respiration and heartbeat, based on microwave Doppler phase modulation effect has been studied for many years [1], [2]. To achieve an accurate and robust performance, researchers in recent years have been working to further explore several technical challenges [3]–[10]. As one of the main challenges, the null detection point problem was solved by the frequency tuning technique [4] and the arctangent demodulation [6]. However, the frequency tuning technique requires tuning the intermediate frequency once the distance between the antenna and the subject changes; and the reported arctangent demodulation requires calibration of the baseband dc offset [6]. Unfortunately the dc offset for noncontact vital sign detection is not only produced by the electronic components, but also by the unmodulated reflected signal, i.e., signal reflected from stationary objects and other parts of the human body rather than the moving chest wall. Therefore, the dc offset calibration is more than just calibrating the receiver chain. It is required once the experimental environment changes. Recently, a complex signal demodulation technique was proposed [8] for noncontact vital sign detection. This technique can reliably eliminate the null detection point problem at a low cost. Moreover, since the objective of vital sign detection is to identify the frequency of the desired signal components, which are not related to the dc component, the complex signal demodulation does not need dc offset information when no random body movement is present.

In addition to the experimental efforts to improve the system performance, theoretical analyses have been performed to study the Doppler noncontact vital sign detection and provide guidelines for the designs. Achievements include the analysis on the range correlation effect and I/Q performance benefits [3], the modeling and analysis of the double-sideband transmission to eliminate the null detection point [4], the spectral analysis of nonlinear phase modulation effect [5], the analysis of the arctangent demodulation in quadrature receivers [6], and the comparative study on different radio architectures for vital sign detection [9].

However, the distinctive properties of noncontact vital sign detection still require further attention in the following aspects. First, noncontact vital sign sensing is based on detecting the periodic phase change. Since the detection is typically carried out within a few meters, the phase offset accumulated in the transmission path varies significantly from one path to another, making the detection potentially sensitive to the near field effect [11], [12].

Moreover, since the noncontact vital sign detection is based on sensing the small physiological movement in millimeter or centimeter range, the presence of random body movement produces a significant source of noise for the accurate detection. Although successful Doppler radar noncontact vital sign detection under different environment for different applications has been reported in the past two decades [1]–[6], a critical issue that prevents this technology from being widely used is the noise produced by random body movement. For example, when the radar was used for overnight monitoring of sleep apnea in clinical environment, the detected vital sign signal will be interrupted when the subject under test is rolling over on the bed, producing false alarm. It is recently reported in [8] that the random body movement can be cancelled out by detecting from both the front and the back of the human body using complex signal demodulation. This cancellation technique can be widely adopted for applications such as sleep apnea monitor, lie detector, and baby monitor. In these applications, two identical portable radars can be conveniently implemented under and above the bed, or at a distance from the front and the back of a seated subject.

In this paper, in addition to the reported complex signal demodulation used for random body movement cancellation [8], another important demodulation method of noncontact vital sign detection, i.e., the arctangent demodulation, is also

Manuscript received April 24, 2008; revised July 09, 2008. First published November 18, 2008; current version published December 05, 2008.

The authors are with the Department of Electrical and Computer Engineering, University of Florida, Gainesville, FL 32611 USA (e-mail: changzhi@ufl.edu; jenshan@ufl.edu).

Color versions of one or more of the figures in this paper are available online at http://ieeexplore.ieee.org.

Digital Object Identifier 10.1109/TMTT.2008.2007139

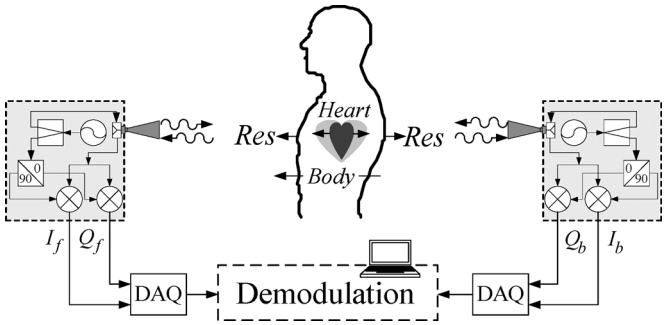

Fig. 1. Simplified block diagram for Doppler radar noncontact vital sign detection.

studied for random body movement cancellation. It is shown that if the baseband dc offset information is known, both of the two demodulation techniques can be used for random body movement cancellation. When the dc offset cannot be accurately calibrated out, the complex signal demodulation is more favorable for random body movement cancellation. The *ray-tracing model* used in the study will also show for the first time the effects of *constellation deformation* and *optimum/null detection ambiguity* caused by the phase offset due to finite antenna directivity.

The two demodulation techniques and their implementation for random body movement cancellation are studied in Section II. The effect of phase offset is discussed in Section III. Simulations have been performed and the results are reported in Section IV. Experimental results are presented in Section V, and a conclusion is drawn in Section VI.

II. Complex Signal Demodulation and Arctangent Demodulation

Fig. 1 shows the block diagram for Doppler radar noncontact vital sign detection. The measurement can be performed from either the front or the back of the human body. When random body movement is present and it affects accurate detection, the measurement has to be performed simultaneously from both sides to cancel out the random frequency drift [8].

In the analysis of noncontact quadrature demodulation of vital sign, the *single-beam model* assumes an ideal antenna with infinite directivity focusing a beam at the location of the heart. When no random body movement is present, the normalized detected baseband signal in one of the baseband I/Q channels can be represented and analyzed by spectral analysis as [10]

$$\begin{aligned} B(t) &= \cos\left(\frac{4\pi x_h(t)}{\lambda} + \frac{4\pi x_r(t)}{\lambda} + \phi\right) \\ &= \sum_{k=-\infty}^{\infty}\sum_{l=-\infty}^{\infty} J_l\left(\frac{4\pi m_h}{\lambda}\right) J_k\left(\frac{4\pi m_r}{\lambda}\right) \\ &\quad \cdot \cos(k\omega_r t + l\omega_h t + \phi) \end{aligned} \tag{1}$$

where $x_h(t) = m_h \cdot \sin\omega_h t$, $x_r(t) = m_r \cdot \sin\omega_r t$ are the periodic body movements due to heartbeat and respiration, λ is the wavelength of the wireless signal, ϕ is the total residual phase accumulated in the circuit and along the transmission path, and J_n is the Bessel function of the first kind.

For a quadrature transceiver, the baseband output in the I/Q channel can be represented as $B(t)$ and the quadrature of $B(t)$. Meanwhile, the Bessel coefficient with a negative index number and a positive index number in (1) can be combined using the property: $J_n(x) = J_{-n}(x)$ for even numbers of n and $J_n(x) = -J_{-n}(x)$ for odd numbers of n. Therefore, the baseband I/Q output can be represented as

$$\begin{aligned} I(t) &= \cos\left(\frac{4\pi x_h(t)}{\lambda} + \frac{4\pi x_r(t)}{\lambda} + \phi\right) \\ &= \mathrm{DC}_I - 2\left[C_{10}\sin(\omega_r t) + C_{01}\sin(\omega_h t) + \cdots\right]\cdot\sin\phi \\ &\quad + 2\left[C_{20}\cos(2\omega_r t) + C_{02}\cos(2\omega_h t) + \cdots\right]\cdot\cos\phi \end{aligned} \tag{2a}$$

$$\begin{aligned} Q(t) &= \sin\left(\frac{4\pi x_h(t)}{\lambda} + \frac{4\pi x_r(t)}{\lambda} + \phi\right) \\ &= \mathrm{DC}_Q + 2\left[C_{10}\sin(\omega_r t) + C_{01}\sin(\omega_h t) + \cdots\right]\cdot\cos\phi \\ &\quad + 2\left[C_{20}\cos(2\omega_r t) + C_{02}\cos(2\omega_h t) + \cdots\right]\cdot\sin\phi \end{aligned} \tag{2b}$$

where $C_{ij} = J_i(4\pi m_r/\lambda)\cdot J_j(4\pi m_h/\lambda)$ determines the amplitude of every frequency component, $\mathrm{DC}_I = J_0(4\pi m_r/\lambda)\cdot J_0(4\pi m_h/\lambda)\cdot\cos\phi$ and $\mathrm{DC}_Q = J_0(4\pi m_r/\lambda)\cdot J_0(4\pi m_h/\lambda)\cdot\sin\phi$ are the dc components of the signals in I and Q channels, respectively. The ellipses in (2) represent higher order odd and even harmonics. It should be noted that DC_I and DC_Q are the dc information directly related to the physiological movement. As will be shown in the following sections, they are beneficial for the recovering of vital sign signals in some cases and thus can be defined as the "desired dc information." In real experiment, due to the dc offset caused by the signals reflected from environmental stationary objects (clutter) and the dc offset accumulated in the electronic circuit, the measured baseband dc level is the $\mathrm{DC}_I/\mathrm{DC}_Q$ level plus an 'undesired dc offset'.

From (2), the ratio of $\cos\phi$ and $\sin\phi$ determines the relative strength between the even order and the odd order harmonics. Therefore, the optimal/null detection point is determined by the residue phase ϕ. For example, when ϕ is close to 90°, the fundamental frequency of respiration and heartbeat signals dominates in the I channel while the second order harmonic of desired signals dominates in the Q channel, thus I is close to the optimal detection point and Q is close to the null detection point. According to the *single-beam model*, when either one of the two quadrature channels is close to an optimal detection point, the other one should be close to the null detection point.

A. Complex Signal Demodulation

The complex signal demodulation can eliminate the optimum/null detection point problem by combining the I and Q signals in baseband. As shown in Fig. 2(a), the complex signal is software-reconstructed in real time as

$$\begin{aligned} S(t) &= I(t) + j\cdot Q(t) \\ &= \exp\left\{j\left[\frac{4\pi x_h(t)}{\lambda} + \frac{4\pi x_r(t)}{\lambda} + \phi\right]\right\} \\ &= \mathrm{DC}_{IQ} + 2j\left[C_{10}\sin(\omega_r t) + C_{01}\sin(\omega_h t) + \cdots\right]\cdot \mathrm{e}^{j\phi} \\ &\quad + 2\left[C_{20}\cos(2\omega_r t) + C_{02}\cos(2\omega_h t) + \cdots\right]\cdot \mathrm{e}^{j\phi} \end{aligned} \tag{3}$$

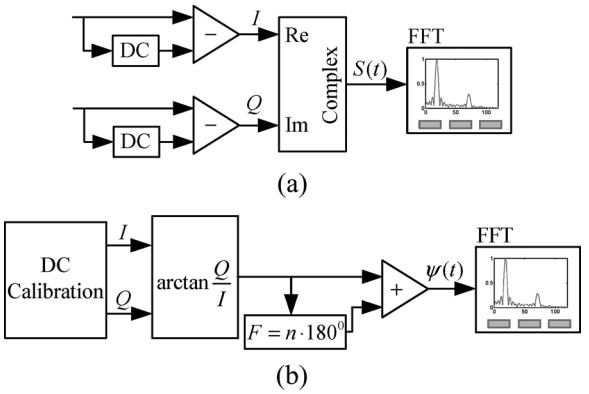

Fig. 2. Block diagram of complex signal: (a) demodulation and (b) arctangent demodulation.

where $\mathrm{DC}_{IQ} = \mathrm{DC}_I + j \cdot \mathrm{DC}_Q$. Since $\mathrm{e}^{j\phi}$ has a constant envelope of one, the effect of ϕ on signal amplitude can be eliminated. Applying the complex Fourier transform to the signal $S(t)$ for spectral analysis, the residual phase ϕ will not affect the relative strength between the odd order and the even order frequency components. The desired signal components (odd order tones) will always be present in the spectrum.

Meanwhile, even though dc offsets exist in the I/Q channels and may lead to the error of measured $\mathrm{DC}_I/\mathrm{DC}_Q$, they only affect the dc term of $S(t)$, i.e., DC_{IQ} in (3). Therefore, the existence of dc offset does not affect obtaining the frequency of the desired signal components. In practice, the residual baseband dc level, which is a sum of the physiological-movement-related $\mathrm{DC}_I/\mathrm{DC}_Q$ and the dc offset, can be easily extracted as the average of signals in every time-domain sliding window and thus be safely removed. As a result, the complex signal demodulation greatly simplifies the demodulation procedure and is immune from dc offset when no random body movement is present. However, the complex signal demodulation is not able to completely eliminate the higher even order harmonics.

For random body movement cancellation, measurements need to be performed from both sides of the human body. In this way, the signal detected from the two transceivers can be expressed as

$$S_f(t) = \exp\left\{ j \left[\frac{4\pi x_{h1}(t)}{\lambda} + \frac{4\pi x_{r1}(t)}{\lambda} + \frac{4\pi y(t)}{\lambda} + \phi_1 \right] \right\} \quad (4a)$$

$$S_b(t) = \exp\left\{ j \left[\frac{4\pi x_{h2}(t)}{\lambda} + \frac{4\pi x_{r2}(t)}{\lambda} - \frac{4\pi y(t)}{\lambda} + \phi_2 \right] \right\} \quad (4b)$$

where $x_{h1}(t)$ and $x_{r1}(t)$ are the heartbeat- and respiration-induced physiological movements on the front chest wall, $x_{h2}(t)$ and $x_{r2}(t)$ are the heartbeat-induced and the respiration-induced physiological movements on the back, ϕ_1, ϕ_2 are the residual phase of the transceivers in front of the body and behind the body, and $y(t)$ is the random body movement. Note that the pairs of physiological movements on both sides of the body, e.g., $x_{h1}(t)$ and $x_{h2}(t)$, move in the same direction relative to their respective detecting radar. On the other hand, when the body is drifting toward one of the radars, it is moving away from the other one. Therefore, by multiplying $S_f(t)$ and $S_b(t)$, the $y(t)$ term in the baseband output $S_{fb}(t) = S_f(t) \cdot S_b(t)$ will be cancelled out, while the physiological movement terms are enhanced as follows:

$$S_{fb}(t) = \exp\left\{ j \left[\frac{4\pi \left[x_{h1}(t) + x_{h2}(t) \right]}{\lambda} + \frac{4\pi \left[x_{r1}(t) + x_{r2}(t) \right]}{\lambda} + \phi_1 + \phi_2 \right] \right\}. \quad (5)$$

The above operation can also be interpreted as convolution and frequency shift in frequency domain, thus canceling the Doppler frequency drift and keeping only the periodic Doppler phase effects.

Although it is shown that the complex signal demodulation itself does not require the dc information and is immune to the dc offset, the performance of random body movement cancellation is affected by the dc offset. Proper estimation or calibration of the dc offset is beneficial for successful cancellation of the noise due to random body movement.

B. Arctangent Demodulation

Another way to eliminate the optimum/null detection point problem in the quadrature demodulation system is to use arctangent demodulation [6] by calculating the total Doppler phase shift. Its block diagram is shown in Fig. 2(b). Taking into account the phase discontinuity when the signal trajectory crosses the boundary of two adjacent quadrants, the arctangent demodulation calculates the total angular information $\psi(t)$ as

$$\psi(t) = \arctan \frac{Q(t)}{I(t)} + F = \frac{4\pi x_h(t)}{\lambda} + \frac{4\pi x_r(t)}{\lambda} + \phi \quad (6)$$

where F is a multiple of 180° for the purpose of eliminating the discontinuity when $\psi(t)$ crosses the boundary of two adjacent quadrants in the constellation graph.

Since $\psi(t)$ is a linear combination of the desired signal $x_h(t)$ and $x_r(t)$, the information of the vital signs can be obtained with the nonlinear phase modulation effect eliminated. The advantage is the ability to eliminate the harmonic and intermodulation interference. However, previous demonstration [6] of this technique requires accurate calibration of the dc offset in order to properly reconstruct the angular information. The difficulty of accurate dc offset calibration encountered in Doppler radar vital sign detection is that the dc offset is not only produced by the electronic circuit, but also by the unmodulated reflected signal, i.e., signal reflected from stationary objects and other parts of the human body rather than the moving chest wall. Therefore, the dc offset changes as the environment changes and needs to be calibrated when it is changed [6].

On the other hand, the presence of baseband dc offset results in an error in $\mathrm{DC}_I/\mathrm{DC}_Q$ defined in (2). This leads to a shifted trajectory in the constellation graph. Although the angular information $\psi(t)$ will be changed significantly when the trajectory is shifted, the angular movement is still periodic. This implies that when analyzing the spectrum of $\psi(t)$ in the presence of a dc offset, the desired frequency components still exist. The difference observed in the spectrum is a changed harmonic level. Therefore, if the dc offset can be properly estimated, it is still

possible to extract the desired vital signs without a dc offset calibration. As will be demonstrated in Section V, a trajectory-fitting procedure is adopted in this paper for dc offset estimation in the baseband. Experiments will show that this procedure can be used for vital sign detection in the absence of random body movement.

When random body movement is present, the angular information recovered from the front (ψ_f) and the back (ψ_b) of the human body can be expressed as

$$\psi_f(t) = \frac{4\pi x_{h1}(t)}{\lambda} + \frac{4\pi x_{r1}(t)}{\lambda} + \frac{4\pi y(t)}{\lambda} + \phi_1 \quad (7a)$$

$$\psi_b(t) = \frac{4\pi x_{h2}(t)}{\lambda} + \frac{4\pi x_{r2}(t)}{\lambda} - \frac{4\pi y(t)}{\lambda} + \phi_2 \quad (7b)$$

where $x_{h1}(t)$, $x_{r1}(t)$, $x_{h2}(t)$, $x_{r2}(t)$, ϕ_1, and ϕ_2 are the same as defined in Section II-A. Instead of multiplying the two signals as in the case of using complex signal demodulation, the random body movement can be cancelled out by adding the angular information of (7a) and (7b) together to obtain $\psi_{fb}(t) = \psi_f(t) + \psi_b(t)$ as follows:

$$\psi_{fb}(t) = \frac{4\pi\,[x_{h1}(t)+x_{h2}(t)]}{\lambda} + \frac{4\pi\,[x_{r1}(t)+x_{r2}(t)]}{\lambda} + \phi_1 + \phi_2. \quad (8)$$

As a result, the Doppler frequency drift caused by the random movement of $y(t)$ is eliminated, leaving only the desired frequency components in the spectrum of $\psi_{fb}(t)$.

The critical issue of using arctangent demodulation for random body movement cancellation is how the presence of the baseband dc offset will affect the detection. As will be shown in simulation and experiments, the complex signal demodulation is more favorable for random body movement cancellation when the dc offset cannot be accurately determined and calibrated.

III. Effects of Phase Offset

Since a real antenna with a certain radiation pattern does not have infinite directivity, signals are reflected and captured from different parts of the body. When signals on different paths with different intensity and residual phases are received by the radar, they are simply summed together by the receiving antenna, either canceling out or enhancing the desired signal components. Therefore, a *ray-tracing model* [9] is developed to compensate for the shortage of the *single-beam model*.

As shown in Fig. 3(a), the actual received signal should be represented from a ray-tracing point of view as

$$I(t) = \iint_s E(x,y) \cdot \cos\left[\left[\Delta\phi + \frac{4\pi}{\lambda}\left\{\rho(x,y)^2 + [d_0 + m_h(x,y)\sin(\omega_h t) + m_r(x,y)\sin(\omega_r t)]^2\right\}^{1/2}\right]\right] \times ds \quad (9a)$$

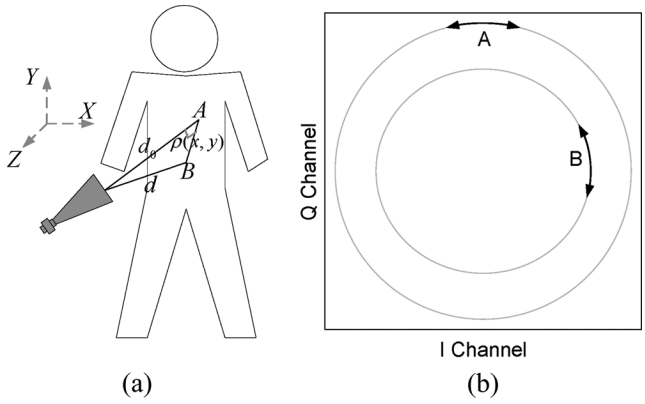

Fig. 3. (a) Ray-tracing model and (b) the angular information of signals reflected from point A and B on the body using a 5.8 GHz radar. The antenna is facing the body in the $-Z$ direction of the $X - Y - Z$ coordinate.

$$Q(t) = \iint_s E(x,y) \cdot \sin\left[\left[\Delta\phi + \frac{4\pi}{\lambda}\left\{\rho(x,y)^2 + [d_0 + m_h(x,y)\sin(\omega_h t) + m_r(x,y)\sin(\omega_r t)]^2\right\}^{1/2}\right]\right] \times ds. \quad (9b)$$

where $E(x,y)$ is the intensity of the electromagnetic wave reflected from the location (x,y) of the human body, d_0 is the distance between the antenna and the subject under test, $\rho(x,y)$ is the distance between location (x,y) and the antenna's projection on the chest wall, and $\Delta\phi$ is the residual phase shift accumulated in the electronic circuit. The integration is carried out over the entire subject under test.

Assume the antenna is placed 1 m away in front of the heart center, and the locations of the heart center A and the body center B on the front chest wall are separated by 11 cm. The difference in the transmission path for signals from the antenna to the two points is $\Delta x = \sqrt{1^2 + 0.11^2} - 1 = 0.006$ m, which is replicated in the receiving path and would produce a phase difference of 83.5 degree for a 5.8 GHz radar. Meanwhile, the radiation intensity of the antenna on the body surface is different from point to point, depending on the antenna radiation pattern. This implies that the received baseband signals from the two points will have different locations and movement patterns in the constellation graph, as shown in Fig. 3(b). Therefore, the real case for vital sign detection using complex signal demodulation and arctangent demodulation is complicated by the phase offset. Numerical simulations are needed and will be presented in the following section.

IV. Simulation

Simulations have been performed based on the *ray-tracing model*. The two demodulation techniques were applied to vital sign detection in the presence/absence of random body movement.

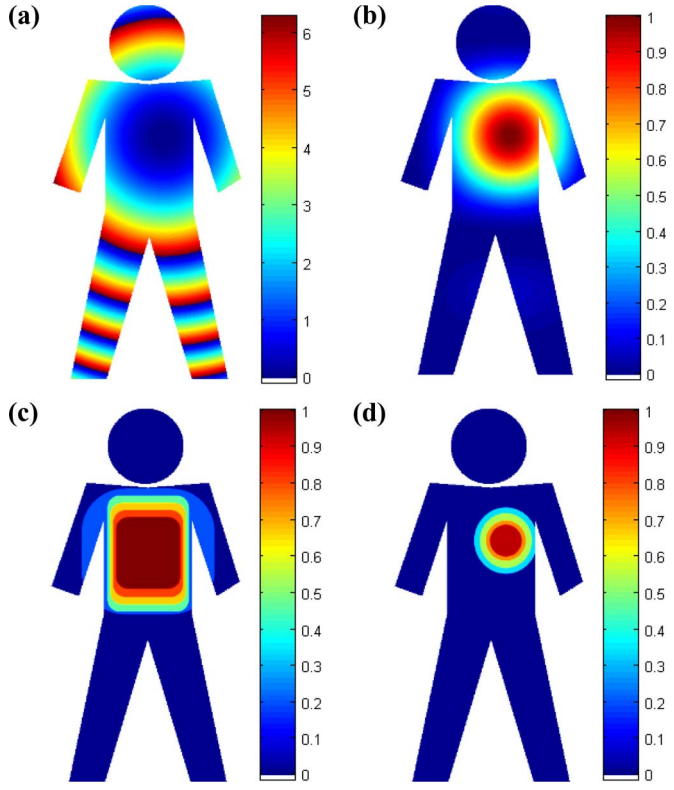

Fig. 4. Ray-tracing model. (a) Phase offset on the surface of human body radiated by a 5.8 GHz radar. (b) 7 by 7 elements antenna array's radiation intensity on the human body. (c) Approximation of the normalized amplitude of body movement caused by respiration. (d) Approximation of the normalized amplitude of body movement caused by heartbeat.

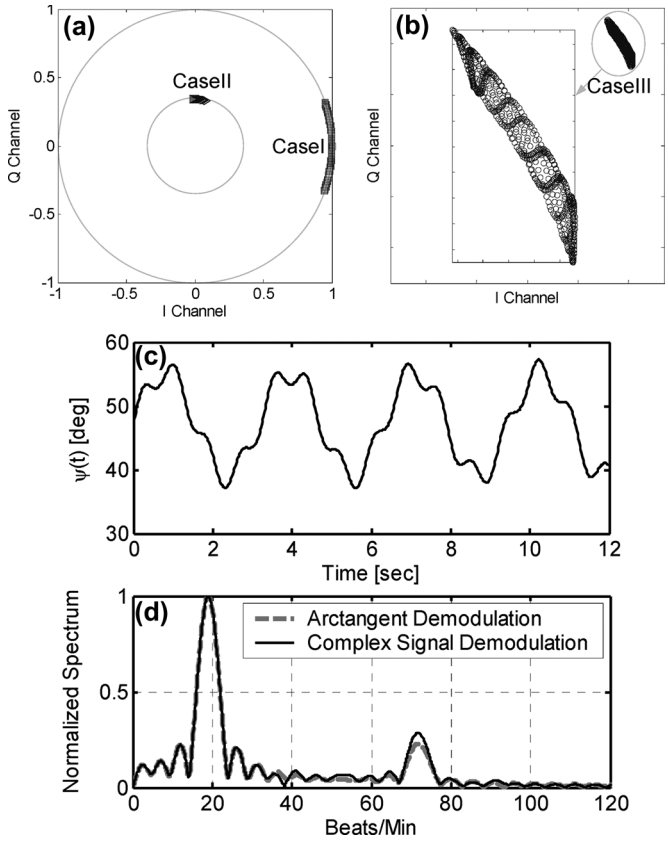

Fig. 5. Demodulation for a 5.8 GHz radar. (a) Signal detected at heart center (Case I) and at body center (Case II). (b) Actual received signal (Case III). (c) Angular information $\psi(t)$ of the received signal. (d) Baseband spectra obtained by the complex signal demodulation and the arctangent demodulation (the dc component is not shown in the baseband spectrum).

A. Ray-Tracing Model

The body model for a subject of 1.8 m height is shown in Fig. 4. Assuming the antenna is 1 m in front of the heart center, the phase offset in different paths compared with the beam propagating to the center of the heart is shown in Fig. 4(a) for a 5.8 GHz radar sensor. Dramatic change in phase offset is observed. Shown in Fig. 4(b) is the radiation intensity on the human body produced by an ideal 7 by 7 antenna array comprised of omnidirectional antennas spaced by $\lambda/2$. Fig. 4(c) and (d) are the approximation of the normalized amplitude of body movements caused by respiration and heartbeat, respectively. It can be inferred that when a carrier frequency of 24 GHz is used for the higher sensitivity at shorter wavelengths, the phase change will be more significant.

B. Demodulation Without Random Body Movement

To demonstrate the properties of the two demodulation techniques, numerical simulations were first performed without random body movement present. Two examples are presented, i.e., a 5.8 GHz quadrature radar, and a 24 GHz quadrature radar. The following three types of signals were recorded and analyzed.

- Case I: A single-beam signal projected to the heart center, i.e., point A in Fig. 3. This is the case analyzed by the *single-beam model*.
- Case II: A single-beam signal projected to the body center, i.e., point B in Fig. 3. In this case, respiration signal was picked up while heartbeat signal is almost absent.
- Case III: The actual signal transmitted and received by the radar.

It should be noted that only Case III can be realized in the laboratory. Case I and II analyze signals carried by a hypothetical single beam radiated by an antenna with a very high directivity radiation pattern.

Example I: 5.8 GHz Quadrature Radar: Simulation results are shown in Fig. 5 for detection from the back of the human body. The residual phase produced in the electronic circuit was assumed to be 0°, which means the Q channel was at the optimum detection point while the I channel was at the null detection point according to the single-beam model.

Fig. 5(a) and (b) shows the signal trajectories in the constellation graph. As predicted in Section II, signals reflected from different parts of the human body are affected by two variations: the phase offset and the radiation intensity. The former variation embodies itself as different angles of the trajectory shown in Fig. 5(a), while the latter is demonstrated as different radii of the trajectory. As a result, when the receiver receives the vital sign signals, which is the superposition of all the signals reflected from different parts of the body, the total received signal trajectory is deformed from an ideal circle, as shown in Fig. 5(b). It

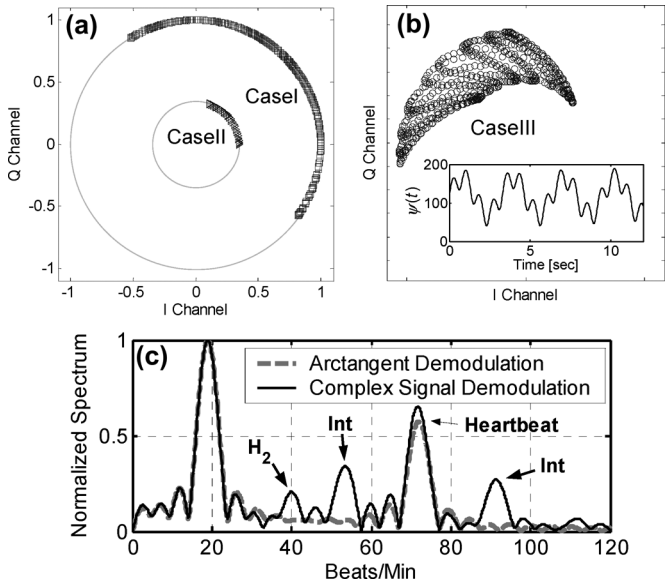

Fig. 6. Demodulation for a 24 GHz radar. (a) Signal detected at heart center (Case I) and at body center (Case II). (b) Actual received signal (Case III), with the recovered angular information shown in inset. (c) Baseband spectra obtained by the complex signal demodulation and the arctangent demodulation (dc component not shown in the spectra). The complex signal demodulation causes harmonic (H_2) and intermodulation (Int) interference.

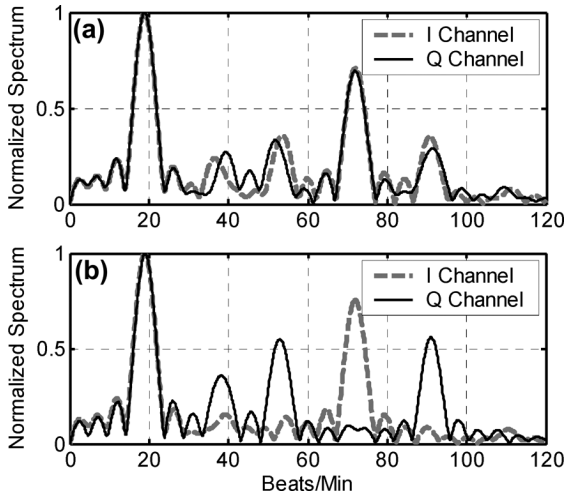

Fig. 7. Baseband spectrum detected by the I and the Q channels with a carrier frequency of 24 GHz. (a) Spectrum of a single-beam signal projected to the heart center. (b) Spectrum of the actually received signal.

should be noted that the *constellation deformation* is not caused by noise, which was not included in simulation.

Although the foregoing discussions and simulation results appear undesirable, the recovered angular information based on (6) is nonetheless periodic and not seriously disturbed by the phase offset problem, as shown in Fig. 5(c). The spectrum of the complex signal and the recovered angular information were analyzed and plotted in Fig. 5(d). Although the detection was made with one channel at the null detection point and the other at the optimum detection point, both of the two demodulation techniques can successfully identify the respiration and heartbeat components.

Therefore, the complex signal demodulation and the arctangent demodulation for 5.8 GHz radar system are demonstrated to be effective solutions to achieve reliable detection and eliminate the null detection point problem.

Example II: 24 GHz Quadrature Radar: In this example, the carrier frequency was 24 GHz and the residual phase produced in the electronic circuit was assumed to be 45°, which means the detection was performed at the middle between the null and the optimum detection points. The constellation plots are shown in Fig. 6(a) and (b). Due to fast variation of the phase offset on the surface of the human body, more severe trajectory deformation was observed. However, angular information recovered from (6) is still periodic, as shown in the inset of Fig. 6(b). The baseband spectra from the two demodulation techniques are shown in Fig. 6(c). Again, the respiration and the heartbeat components can be identified from the spectrum by using both of the techniques.

Furthermore, the result in Fig. 6(c) verifies that the arctangent demodulation can eliminate the harmonics and intermodulation terms caused by the nonlinear phase modulation effect, making the spectrum cleaner than that obtained by complex signal demodulation.

Another phenomenon to be noted is the *optimum/null detection ambiguity*. Shown in Fig. 7(a) is the baseband spectrum of the I and the Q channels in Case I, i.e., the spectrum of the single beam signal projected to the center of the heart. The peaks of the respiration and the heartbeat components in I channel have the same amplitudes as those in Q channel, which is in accordance with (2) predicted by the *single-beam model* since the detection was performed at the mid-point between the null and the optimum detection points. However, the baseband spectrum of the actual received signal, as shown in Fig. 7(b), shows that the I and the Q channels have significant differences in the heartbeat signal strength. While the I channel preserves the heartbeat signal, the Q channel shows strong harmonic and intermodulation components. This is because of the enhancement and cancellation among signals with different phase offsets. It demonstrates the necessity of effectively combining the two channels even when the detection is not carried out at the null detection point.

C. Random Body Movement Cancellation

The random body movement cancellation technique was also simulated using the *ray-tracing model* with a carrier frequency of 5.8 GHz. The random roaming of the body was fully modeled in three dimensions (X, Y, and Z) which are defined in Fig. 3. Typically the subject under test has larger random body movements in two dimensions than the third dimension, e.g., the horizontal movements in the X and Z directions are more obvious than the vertical movement in the Y direction for a seated person. Therefore, the time-variant velocity of random body movement was modeled as uniform distribution between 0 and a maximum value of 4 mm/s in the X and the Z directions. The amplitude of random body movement in the Y direction was modeled as 0.1 of that in the other two directions. The movement components in each direction are shown in Fig. 8(a), and the baseband spectra detected from the front and the back using the two demodulation techniques are shown in Fig. 8(b).

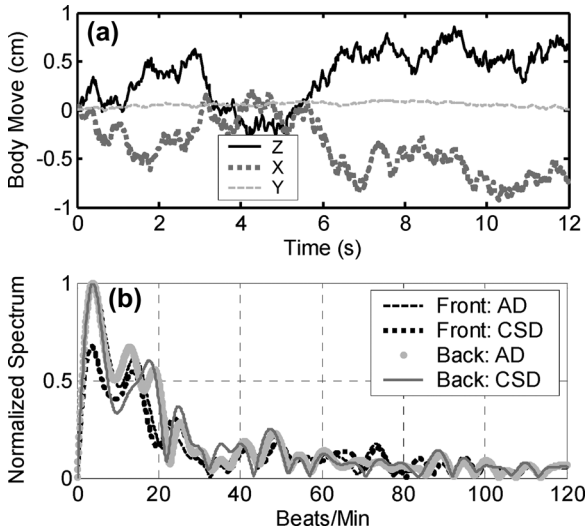

Fig. 8. Baseband spectra obtained when random body movement is present. (a) Random body movement is shown in the Z, X, and Y directions, which are defined in Fig. 3. (b) Baseband spectra by arctangent demodulation (AD) and complex signal demodulation (CSD).

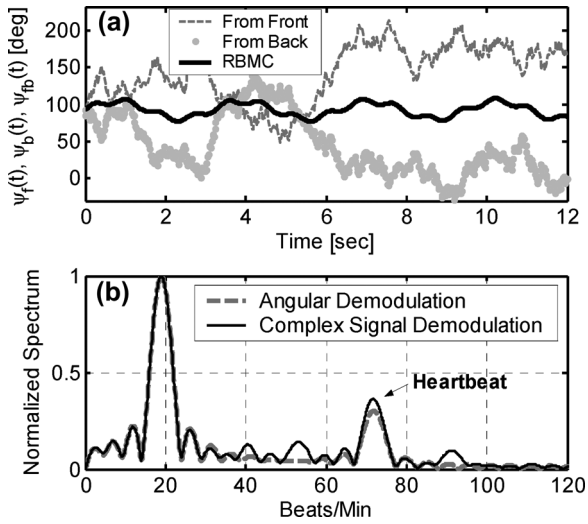

Fig. 9. (a) Angular information and (b) baseband spectrum recovered by random body movement cancellation (RBMC) using the two demodulation techniques; accurate dc information is used in demodulation but not shown in the spectrum.

When random body movement is present, the desired respiration and heartbeat signal components will be overwhelmed by the noise generated by random body movement.

If the system can successfully calibrate out the dc offset up to the baseband output, the recovered baseband angular information and the spectra obtained by random body movement cancellation were simulated and shown in Fig. 9. The respiration and heartbeat components were successfully recovered by both demodulation techniques, which showed similar performance in recovering the desired signal components. It should be noted that although the random body movement can exist in the direction perpendicular to the radar direction, this technique still works reliably because only the movement in the radar direction is critical for the detection.

If the dc offset cannot be perfectly calibrated out up to the baseband output, however, the performance of random body movement cancellation based on both of the demodulation techniques deteriorates. Shown in Fig. 10 is an example when dc offset was present at the baseband output of the two transceivers. For each transceiver, the baseband dc offset levels were modeled to be the same in the I/Q channels and were 30% of the maximum signal amplitude. In the simulation, the above dc offset level was added to the ideal I and Q channel signals. Then, both demodulation techniques were applied to cancel out the random body movement. It is shown that the complex signal demodulation can still identify the respiration and heartbeat components, but the arctangent demodulation is unable to recover the heartbeat signal. The reason for this disadvantage of using arctangent demodulation in random body movement cancellation is, as shown in (8), the cancellation is based on the linear combination of the calculated phase, which is strongly affected by the location of the constellation origin.

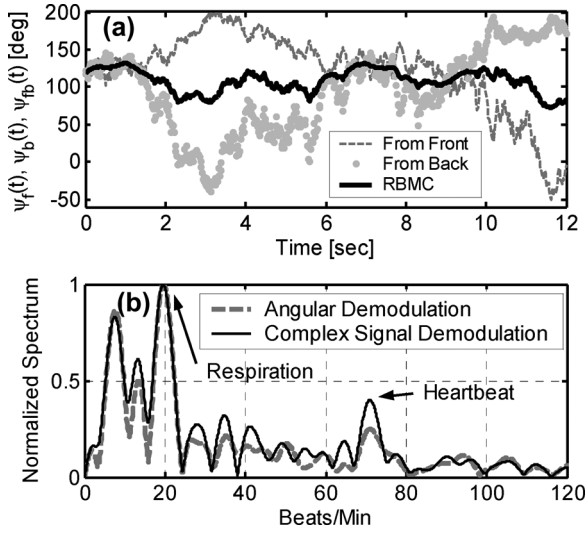

Fig. 10. (a) Angular information and (b) baseband spectrum recovered from the random body movement cancellation (RBMC) technique; the random body movements are modeled in three dimensions, and the dc offset in each transceiver is 30% of the maximum signal amplitude.

V. Experiment

Experiments have been performed in the laboratory to verify the theory and compare the performance of the two demodulation techniques for random body movement cancellation. For consumer applications of this technique, it is desirable to have portable radars that can detect vital signs from several meters away, radiate a power of lower than 0 dBm, and have all the hardware integrated together at an affordable price. Therefore, 4–7 GHz portable radar was designed for this purpose. The radar integrates the quadrature transceiver, the two-stage baseband amplifier, and the power management circuit on a single printed circuit board (Rogers RO4350B substrate) with a size of 6.8×7.5 cm^2. Fig. 11 shows the block diagram of the transceiver. The specifications and manufacturers of the radio frequency components are listed in Table I. For research purpose, four voltage controlled oscillators (VCOs) were implemented for a wide tuning range to obtain different optimal carrier frequencies under different environments [10]. When a specific application is known, only one VCO is needed and the SP4T switch can be eliminated to further reduce the cost.

Since the vital sign has a frequency less than several hertz, large coupling capacitors C_1 and C_2 of 10 μF were used to iso-

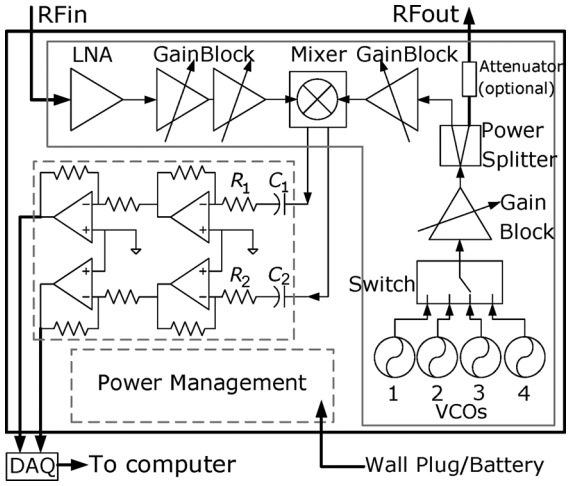

Fig. 11. Block diagram of the 4–7 GHz radar.

TABLE I
BUILDING BLOCKS AND SPECIFICATIONS USED IN 4–7 GHz RADAR

Block	Manufacturer	Specifications
VCO1	Hittite	4.45-5.0 GHz, -105dBc/Hz @100 kHz phase noise, 4 dBm output power
VCO2	Hittite	5.0-5.5 GHz, -103dBc/Hz @100 kHz phase noise, 2 dBm output power
VCO3	Hittite	5.5-6.1 GHz, -102dBc/Hz @100 kHz phase noise, 2 dBm output power
VCO4	Hittite	6.1-6.72 GHz, -101dBc/Hz @100 kHz phase noise, 4.5 dBm output power
Switch	Hittite	DC-8 GHz, 40 dB isolation @6 GHz, 1.8 dB insertion loss @6 GHz, SP4T
Gain Block	RFMD	DC-8 GHz, 15.5 dB maximum gain, 14.5 dBm P1dB @6Ghz
Mixer	Hittite	4-8.5 GHz, 50 dB LO to RF isolation, 40 dB image rejection
LNA	Hittite	3.5-7.0 GHz, 16 dB gain, 2.5 dB NF

late the dc voltages of the mixer output and baseband amplifier input. Because the 10 μF coupling capacitors block the dc signal in addition to isolating dc voltages of two different circuits, a variable dc offset was inevitably introduced into the measurement. The coupling capacitor $(C_1, C_2 = 10\ \mu\text{F})$ and the baseband amplifier input resistor $(R_1, R_2 = 160\ \text{k}\Omega)$ were chosen such that for a heartbeat signal with a frequency around 1 Hz, the voltage drop on the capacitor is no more than 1/10 of the signal amplitude. This leads to a time constant of approximately 1.6 s, which means that in the real-time signal processing software, a 2 s initiation time is needed.

For random body movement cancellation, measurements were performed by two identical radars. As shown in Fig. 12, patch antenna arrays with orthogonal polarization were installed in the two transceivers to eliminate the interference between the two units. It was observed in the experiment that the antenna gain should be higher than 4 dB for the radar to have a good signal-to-noise ratio from up to 2 m away. The antenna was designed to have a maximum directivity gain of 9 dB at broadside, so that the vital signs of the subject in front of the antenna will be picked up. Free-running VCOs were used for the two transmitters so that the actual carrier wavelengths were close to each other but always had a slight difference in the absence of a phase-locked loop. As a result, the signal from one

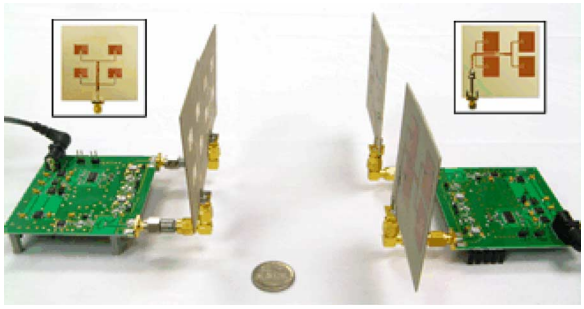

Fig. 12. Two identical transceivers used for random body movement cancellation. Inset: the antenna used for each transceiver. Note that one transceiver uses vertically polarized antenna array, while the other uses horizontally polarized antenna array. From [8].

transceiver was further rejected by the other transceiver in the baseband because the small difference in the carrier frequency results in a large difference in baseband frequency compared to the vital sign frequencies. The phase noise reduction due to range correlation makes the free-running VCO adequate for vital sign detection [3], [13].

To reduce the hardware cost and the requirement of signal processing speed, the amplified baseband signals were sampled by a 12-bit multifunction data acquisition module (NI USB-6008) with a low sampling rate of 20 Hz, which is fast enough for the vital sign signal of typically less than 2.5 Hz. The sampled data were fed into a laptop for real-time signal processing by LabVIEW. The sampling rate and resolution make it possible to implement the baseband signal processing in a low cost DSP microchip such as the TI C2000 family digital signal controllers for various applications in the future.

To focus on the properties of demodulation and random body movement cancellation techniques, no baseband filtering was implemented in either hardware or software. All the results presented are based on the original baseband signal.

A. DC Offset Estimation in Baseband

Due to the coupling capacitor in the radar between the receiver output and the baseband amplifier input and the variability of dc offset within the experimental environment, it is relatively difficult to accurately calibrate out the dc offset of the whole system. Instead, the dc offset was estimated by fitting the signal trajectory into a proper segment of circle in the constellation graph.

For example, Fig. 13(a) shows the constellation graph of the baseband signal detected from the back of the human body when no random body movement was present. Because of the coexistence of the undesired dc offset and the desired dc information, i.e., DC_I/DC_Q in (2), the original signal trajectory was located at the center of the constellation graph. After subtracting an estimated dc offset level of 0.8 V for both the I and Q channels in the baseband, the trajectory was fitted into a circle. Fig. 13(b) shows the baseband spectra obtained by the complex signal demodulation and the arctangent demodulation. As shown in both theory and experiment in [8], the dc offset does not affect complex signal demodulation when random body movement is absent. Therefore, the spectrum obtained by complex signal demodulation can be used as a reference to evaluate the reliability of arctangent demodulation using the estimated dc offset information. The spectra of Fig. 13(b) match well with each other,

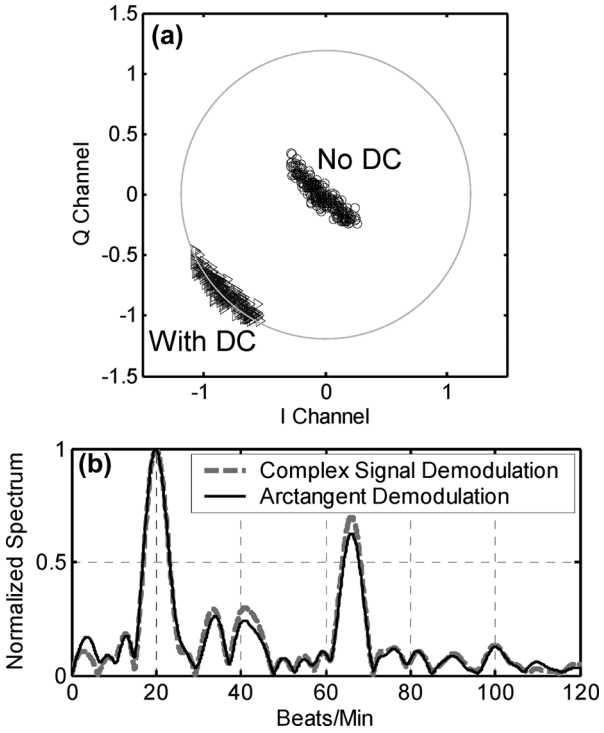

Fig. 13. DC offset estimation. (a) Trajectory of detected baseband signal with no dc information and with estimated dc offset level subtracted. (b) Spectra obtained by the two demodulation techniques. Signal with estimated dc offset subtracted was used for arctangent demodulation.

showing that the baseband dc offset estimation method is accurate enough for arctangent demodulation when no random body movement is present. Based on this dc offset estimation method, estimated dc offsets were subtracted from original detected data and used for random body movement cancellation. However, it should be noted that in the presence of the random body movement, the dc produced by the signals reflected from the bulk of the body always changes. Therefore, it is impossible to dynamically obtain the precise dc offset of the overall system: no matter whether the dc offset is calibrated out using the method proposed in [6] or estimated by the signal trajectory fitting method of this paper, there will always be dc information error when the body position changes. It is of great interest to compare in real experiments that how robust the two demodulation techniques are in the presence of the inevitable dc offset error.

B. Random Body Movement Cancellation

During the experiment, the subject under test was gently changing position in a chair, so that the noise of random body movement was emphasized. Fig. 14 shows the time domain signal detected from the front and the back of the human body when random body movement was present. Since the physiological movement caused by respiration and heartbeat has larger amplitude on the front chest wall than on the back, the signal detected from the back is more severely affected by the random body drift. Note that the detected signal amplitude shown in Fig. 14 does not reflect the real physiological movement amplitude since other factors such as distance and baseband amplifier gain also affect the signal level. For example, in the experiment, the baseband amplifier gain of the radar detecting from the back is 3 dB higher than the other one detecting from

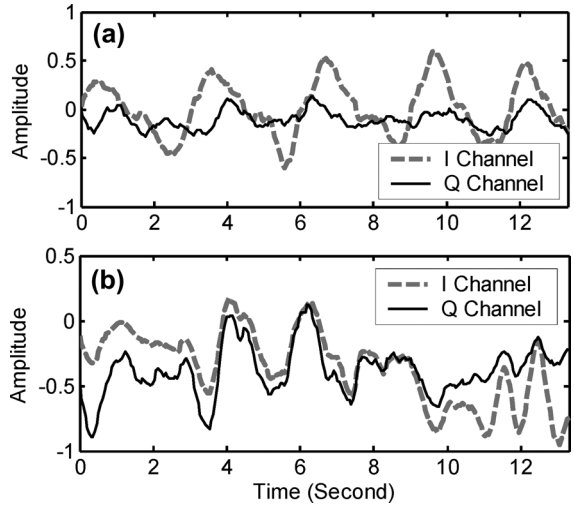

Fig. 14. Signals detected form: (a) the front and (b) the back of human body.

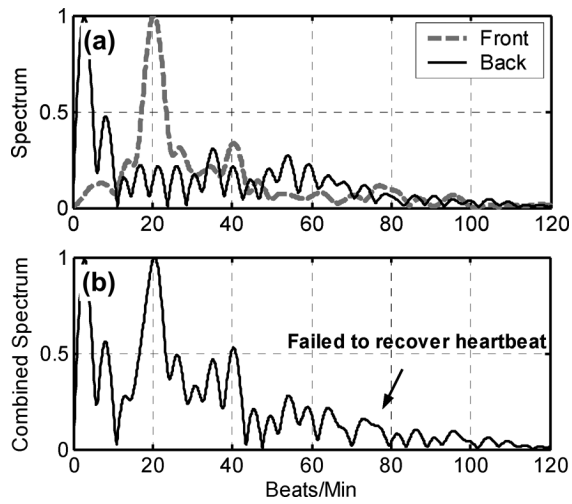

Fig. 15. Random body movement cancellation using arctangent demodulation. (a) Spectra measured from the front and the back of the human body. (b) Spectrum from combining the two transceiver outputs, the heartbeat information cannot be recovered due to inaccurate dc offset information.

the front. The two demodulation techniques were used to cancel out random body movement to recover the desired signal.

The dc offset estimation based on signal trajectory fitting was used here for arctangent demodulation. The baseband spectra detected from the front and the back of the human body are shown in Fig. 15(a). The angular information from the two transceivers was combined as described in Section II-B, and the resulting baseband spectrum is shown in Fig. 15(b). Due to the inaccuracy of dc offset estimation, the combined spectrum failed to recover the desired heartbeat signal component.

On the other hand, the same signals have been processed by the complex signal demodulation. Fig. 16(a) shows the baseband spectra of the complex signal detected from the front and the back of the human body. Since the physiological movement at the back is weaker than that at the front chest wall, the noise completely overwhelmed the physiological signals from the back and only overwhelmed the heartbeat signal from the front. When the technique described in Section II-A was applied to combine the signals detected from the front and the back of

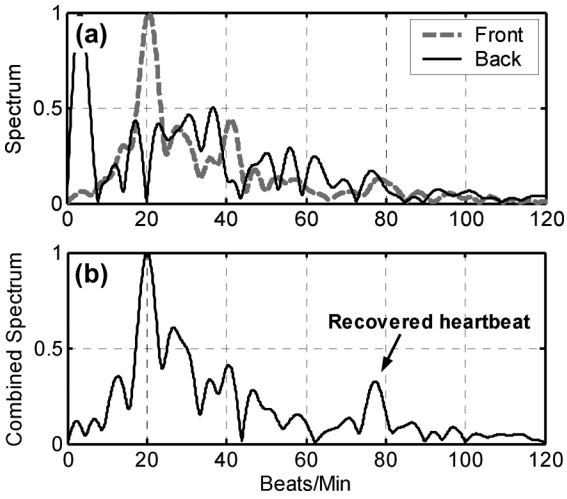

Fig. 16. Random body movement cancellation using complex signal demodulation. (a) Spectra measured from the front and the back of the human body. (b) Output spectrum by the random body movement cancellation technique, the heartbeat information is recovered. From [8].

the human body, the heartbeat signal was successfully recovered as shown in Fig. 16(b).

The above comparative study verifies the simulation in Section IV-C that the complex signal demodulation is more favorable in random body movement cancellation when the dc offset at baseband output cannot be accurately determined.

VI. Conclusion

Simulations and experiments have been performed to demonstrate the complex signal demodulation and the arctangent demodulation for random body movement cancellation in Doppler radar vital sign detection. The complex signal demodulation is easier to implement in that it does not need an intermediate signal processing stage to recover the angular information, and it is robust when dc offset is present. The latter property also makes it more favorable for random body movement cancellation. On the other hand, the arctangent demodulation has the advantage of eliminating the harmonic and intermodulation interference at high frequencies using high gain antennas. The effects of constellation deformation and optimum/null detection ambiguity caused by the phase offset due to finite antenna directivity are also discussed.

Acknowledgment

The authors wish to acknowledge the Hittite Corporation, RFMD, and Rogers Corporation for providing microwave integrated circuits and laminate substrates.

References

[1] J. C. Lin, "Microwave sensing of physiological movement and volume change: A review," *Bioelectromagnetics*, vol. 13, pp. 557–565, 1992.

[2] K. M. Chen, Y. Huang, J. Zhang, and A. Norman, "Microwave life-detection systems for searching human subjects under earthquake rubble and behind barrier," *IEEE Trans. Biomed. Eng.*, vol. 47, no. 1, pp. 105–114, Jan. 2000.

[3] A. D. Droitcour, O. Boric-Lubecke, V. M. Lubecke, J. Lin, and G. T. A. Kovac, "Range correlation and I/Q performance benefits in single-chip silicon Doppler radars for noncontact cardiopulmonary monitoring," *IEEE Trans. Microw. Theory Tech.*, vol. 52, no. 3, pp. 838–848, Mar. 2004.

[4] Y. Xiao, J. Lin, O. Boric-Lubecke, and V. M. Lubecke, "Frequency tuning technique for remote detection of heartbeat and respiration using low-power double-sideband transmission in Ka-band," *IEEE Trans. Microw. Theory Tech.*, vol. 54, no. 5, pp. 2023–2032, May 2006.

[5] C. Li, Y. Xiao, and J. Lin, "Experiment and spectral analysis of a low-power Ka-band heartbeat detector measuring from four sides of a human body," *IEEE Trans. Microw. Theory Tech.*, vol. 54, no. 12, pp. 4464–4471, Dec. 2006.

[6] B. Park, O. Boric-Lubecke, and V. M. Lubecke, "Arctangent demodulation with DC offset compensation in quadrature Doppler radar receiver systems," *IEEE Trans. Microw. Theory Tech.*, vol. 55, pp. 1073–1079, May 2007.

[7] B. Park, V. M. Lubecke, O. Boric-Lubecke, and A. Host-Madsen, "Center tracking quadrature demodulation for a Doppler radar motion detector," in *IEEE MTT-S Int. Microw. Symp. Dig.*, Jun. 2007, pp. 1323–1326.

[8] C. Li and J. Lin, "Complex signal demodulation and random body movement cancellation techniques for non-contact vital sign detection," in *IEEE MTT-S Int. Microw. Symp. Dig.*, Atlanta, GA, Jun. 2008, pp. 567–570.

[9] C. Li, Y. Xiao, and J. Lin, "Design guidelines for radio frequency non-contact vital sign detection," in *Proc. 29th Annu. Int. IEEE EMBS Conf.*, Lyon, France, Aug. 23–26, 2007, pp. 1651–1654.

[10] C. Li and J. Lin, "Optimal carrier frequency of non-contact vital sign detectors," in *Proc. IEEE Radio Wireless Symp.*, Long Beach, CA, Jan. 9–11, 2007, pp. 281–284.

[11] J. M. Taylor and A. J. Terzuoli, "On the concept of near field radar cross section," in *IEEE AP-S Int. Symp. Dig.*, Jul. 1997, vol. 2, no. 13–18, pp. 1172–1175.

[12] M. I. Skolnik, *Radar Handbook*. New York: McGraw-Hill, 1970.

[13] M. C. Budge, Jr. and M. P. Burt, "Range correlation effects on phase and amplitude noise," in *Proc. IEEE SOUTHEASTCON*, Charlotte, NC, 1993, 5 pp.

Changzhi Li (S'06) received the B.S. degree in electrical engineering from Zhejiang University, Hangzhou, China, in 2004, the M.S. degree in electrical engineering from the University of Florida, Gainesville, in 2007, and is currently working toward the Ph.D. degree in electrical engineering at the University of Florida.

His research interests include biomedical applications of microwave/RF, wireless sensors, and microwave/millimeter-wave circuits.

Mr. Li is a student member of the IEEE Microwave Theory and Techniques Society (IEEE MTT-S). He was the second place recipient of the Best Student Paper Award presented at the 2007 IEEE Radio and Wireless Symposium (RWS), and was a finalist in the 2008 IEEE MTT-S International Microwave Symposium (IMS) Student Paper Competition. He was also the recipient of the 2008 IEEE MTT-S Graduate Fellowship Award.

Jenshan Lin (S'91–M'94–SM'00) received the M.S. and Ph.D. degrees in electrical engineering from the University of California at Los Angeles (UCLA), in 1991 and 1994, respectively.

In July 2003, he joined the University of Florida, Gainesville, as an Associate Professor, and became a Professor in August 2007.

Dr. Lin is an elected IEEE Microwave Theory and Techniques Society (IEEE MTT-S) Administrative Committee (AdCom) member, and a member of its Wireless Communications Technical Committee. He is an associate editor for the IEEE TRANSACTIONS ON MICROWAVE THEORY AND TECHNIQUES. He has served on several conference Steering Committees and Technical Program Committees including the IEEE MTT-S International Microwave Symposium (IMS), Radio Frequency Integrated Circuits Symposium (RFIC), and Radio and Wireless Symposium (RWS). He is currently the Technical Program chair of the 2009 Radio and Wireless Symposium. He was the recipient of the 1994 University of California at Los Angeles (UCLA) Outstanding Ph.D. Award, the 1997 Eta Kappa Nu Outstanding Young Electrical Engineer Honorable Mention Award, and the 2007 IEEE MTT-S. N. Walter Cox Award.